THE JOURNAL OF PHYSICAL CHEMISTRY C

Article

pubs.acs.org/JPCC

Fabrication of Monodispersed Au@SiO_2 Nanoparticles with Highly Stable Silica Layers by Ultrasound-Assisted Stöber Method

José Luis Montaño-Priede,[†] João Paulo Coelho,[‡] Andrés Guerrero-Martínez,*[,‡] Ovidio Peña-Rodríguez,[§] and Umapada Pal*[,†]

[†]Instituto de Física, Benemérita Universidad Autónoma de Puebla, Apdo. Postal J-48, Puebla, Puebla 72570, Mexico

[‡]Departamento de Química Física I, Facultad de Ciencias Químicas, Universidad Complutense de Madrid, 28040 Madrid, Spain

[§]Instituto de Fusión Nuclear, Universidad Politécnica de Madrid, José Gutiérrez Abascal 2, E-28006 Madrid, Spain

Supporting Information

ABSTRACT: Metal@dielectric composite nanostructures are of high demand for their vast technological applications. The Stöber method, either in its original form or by modification, has been utilized for the fabrication of silica shells over metal, semiconductor, or even dielectric nanostructures, with the aim to protect them from degradation, enhance their biocompatibility, or use them for molecular anchoring. However, the stability of silica shells and the dispersion of core−shell nanostructures remain the main limitations for their efficient applications. Here we demonstrate that utilization of ultrasound during hydrolysis and condensation of the metal−organic silicon precursor in Stöber process can produce stable and uniform silica shell layers around gold nanoparticles, enhancing both their stability and dispersion. Through transmission electron microscopy and infrared spectroscopy techniques, we demonstrate that the Au@SiO_2 nanoparticles fabricated with ultrasound treatment during silica shell growth contain a lower content of silanol (Si−OH) groups, which are principally responsible for the instability of silica-coated metal nanostructures. The core−shell structures fabricated by ultrasound-assisted hydrolysis using prefabricated Au nanoparticles are well-dispersed, uniform in size, and protected from further hydrolysis in aqueous media, including simulated body fluid. The method applied to fabricate silica-coated Au nanoparticles can be utilized to fabricate other silica-coated metal nanoparticles to enhance their chemical and thermal stability.

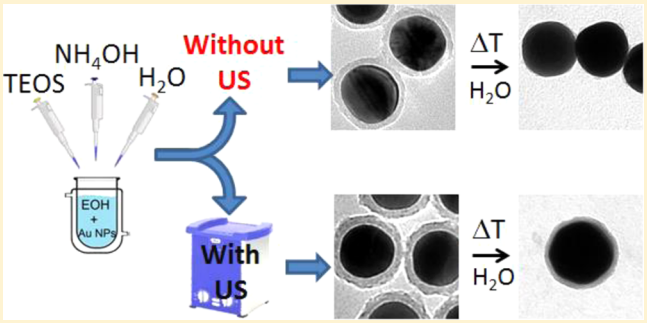

INTRODUCTION

Plasmonic nanostructures coated with dielectric shells have been widely studied for their use in dye-sensitized solar cells (DSSCs),[1−3] shell-isolated nanoparticles-enhanced Raman spectroscopy (SHINERS),[4] and the fabrication of plasmon-enhanced fluorescent devices.[5−7] Both the surface plasmon resonance (SPR) of the plasmonic nanostructures and the physicochemical properties of the dielectric materials such as their optical transparency in the visible spectral region, thermal stability, and chemical inertness have been explored. For most plasmon-enhanced fluorescence applications, SiO_2 is usually chosen as the dielectric shell to protect the metal nanostructures from corrosion and to serve as a molecular anchor, owing to its nontoxicity and facile fabrication via the Stöber method.[8−11] On the contrary, for efficient electromagnetic coupling of surface plasmons with fluorophores to facilitate fluorescence enhancement upon quenching,[10] with the analytes in SHINERS,[12] or for plasmon coupling between metal nanostructures,[4,12] the silica shell thickness should be thin. Silica-coated gold nanoparticles (NPs) have also found applications in biology and medicine. To give a few examples, Au@SiO_2 rattle-type NPs have been utilized for bioimaging and therapeutics.[11] Au-SiO_2 composite NPs and Au nanorods coated with SiO_2 shell have been applied for photoswitched drug delivery in phototherapy.[13−15] Although the optimum silica shell thickness of 2−4 nm and Au NPs of 120−135 nm size range have been seen to produce highest near-field enhancement manifesting the highest surface-enhanced Raman signal,[16] recently we have demonstrated that near-field enhancement in Au@SiO_2 structures depend on both the thickness of the shell layer and the size of plasmonic core.[17]

While fabricating silica shells over metallic nanostructures, we must consider that the affinity of silica with metal surface is low for some metals like gold, and the common stabilizing agents used for fabricating metal nanostructures make them vitreophobic.[18] Therefore, prior to shell fabrication, the metal surface should be functionalized with agents that stabilize the nanostructures and have high affinity to silica. One of the common approaches in this regard is the use of (3-aminopropyl) trimethoxysilane (APS), a silane coupling

Received: January 29, 2017
Revised: April 10, 2017
Published: April 19, 2017

DOI: 10.1021/acs.jpcc.7b00933
J. Phys. Chem. C 2017, 121, 9543−9551

agent. Thin silica shells of 2−4 nm thick could be grown over Au NPs through controlled polymerization of active silica over the metal surface by adding sodium silicate solution to the colloid, maintaining its pH between 10 and 11.[18,19] Nevertheless, the surface of the silica shells fabricated by this method is rough, and the ultimate products are aggregated. The other approach used to fabricate thin silica shells over metal NPs is by modifying the Stöber method.[20] In this method, the metal nanostructures can be functionalized with a thiolated polyether, which also has high affinity to tetraethyl orthosilicate (TEOS), the silica precursor. Hydrolysis and condensation of TEOS over the metal surface lead to the formation of silica shells from a few to hundreds of nanometers in thickness. However, frequently the resulting nanostructures are aggregated, especially in the case of thinner silica shells.[1,10]

Although substantial progress has been made on the fabrication and size control of silica-coated plasmonic nanostructures during the past decade and a half,[21−23] there exists no report in the literature on the stability of the silica shell of those nanostructures, especially in biological or body fluid media. Nevertheless, in 2010, Wong et al. demonstrated that the silica shells fabricated over gold NPs (Au@SiO_2) through the conventional Stöber method are chemically inhomogeneous in their structure and soluble even in hot water due to their low chemical stability.[24] The chemical inhomogeneity of the silica shells fabricated by conventional Stöber method is the result of slow hydrolysis of TEOS, the commonly used silicon precursor, resulting in TEOS derivatives with one to four hydroxyl groups (Figure 1a), and their slow condensation (Figure 1b). These silica shells are formed with a gradient of increasing chemical stability as the TEOS derivatives are gradually deposited and condensed over the Au surface (Figure 2). Therefore, silica shells of a few nanometer thickness fabricated by the conventional Stöber method can be highly unstable in aqueous biological media.

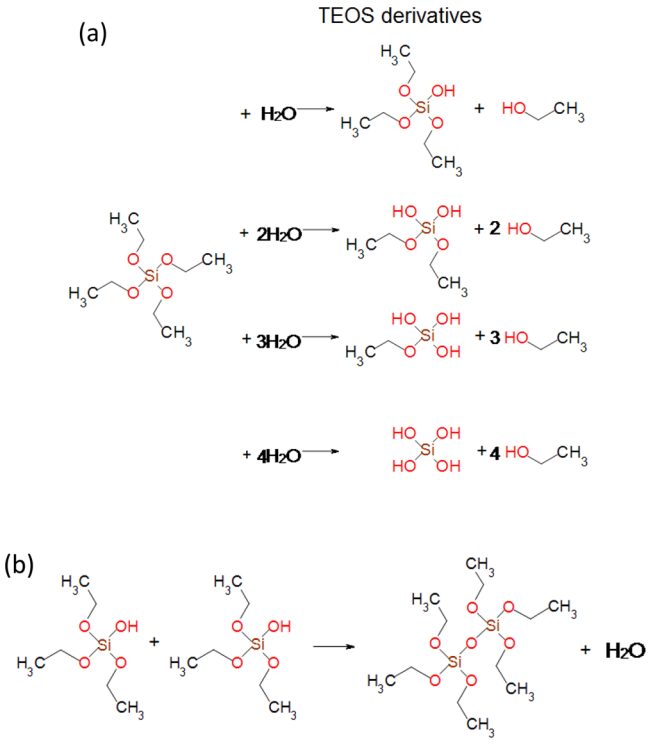

Figure 1. (a) Generation of TEOS derivatives through hydrolysis and (b) condensation of two TEOS derivatives.

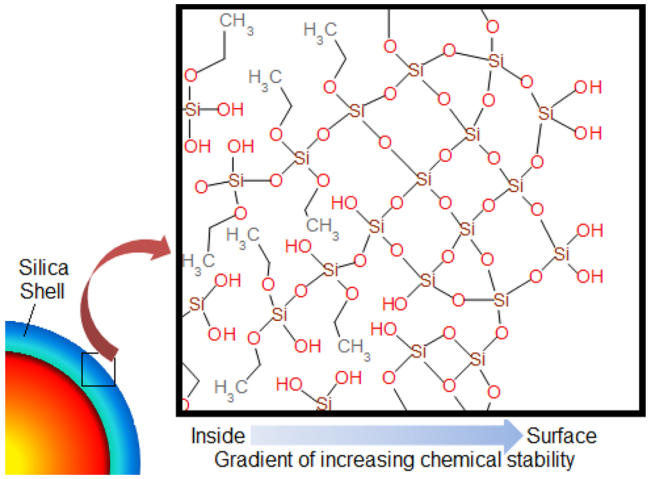

Figure 2. Schematic presentation of the chemical inhomogeneity in a silica shell lattice formed over a metal nanoparticle by the Stöber method.

Wong et al. have also demonstrated that heating the reaction solution during shell fabrication or incubation in a TEOS solution after shell fabrication at 60 °C for 10 h enhances the stability of the silica shells (preventing shell etching).[24] Thermal treatment during shell growth is believed to enhance the cross-linking of the silica matrix, that is, transforming the remaining silanol groups (Si−OH) to siloxane groups (Si−O−Si), causing overall shell hardening.

Although a considerable number of publications on the fabrication and application of silica shell over metal nanostructures exist in the literature,[1,10,19−26] most of them present TEM images as evidence of the formation of core@shell structures without discussing their stability. On the contrary, these composite nanostructures are frequently interconnected or aggregated, especially in the case of thinner silica shells due to their chemical instability.[1,10,18,25,26] Because the optical properties of aggregated NPs are quite different from those of dispersed ones, aggregation processes make them unusable for photonic and biomedical applications.[10,20,27]

In this work, we present a modified Stöber method for the synthesis of thin silica shells over prefabricated monodispersed gold NPs, in which ultrasonic (US) treatment during the TEOS hydrolysis affords more stable silica shells, preventing the aggregation of the Au@SiO_2 NPs during shell formation. The utilized fabrication process produced stable, well-dispersed Au@SiO_2 NPs of uniform size, which are stable not only in hot water but also in simulated body fluid (SBF) media.

EXPERIMENTAL METHOD

Materials. Gold(III) chloride ($HAuCl_4 \cdot H_2O$, 99.999%), sodium borohydride ($NaBH_4$, 99.99%), L-ascorbic acid (AA, ≥99%), cetyltrimethylammonium chloride solution (CTAC, 25 wt % in H_2O), and cetyltrimethylammonium bromide (CTAB, ≥99%) used for the synthesis of gold NPs were purchased from Sigma-Aldrich, Mexico. TEOS (≥99%) and poly(ethylene glycol) methyl ether thiol (mPEG-t, av. M_w = 6000) from Sigma-Aldrich, ammonium hydroxide (NH_4OH, aq. sol. 10−35%) from Quimivita, and absolute ethanol (99.9%) from Scharlau were used for silica shell fabrication.

DOI: 10.1021/acs.jpcc.7b00933
J. Phys. Chem. C 2017, 121, 9543−9551

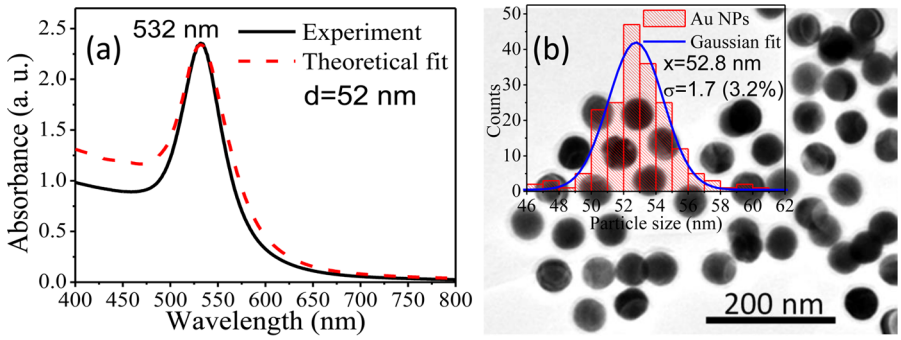

Figure 3. (a) Experimental (black solid line) and theoretical (red dashed line) absorption spectra and (b) a typical TEM image of the as-synthesized gold nanoparticles. Size distribution histogram of the particles is presented as inset.

Sodium hydrogen carbonate ($NaHCO_3$), potassium chloride (KCl), potassium phosphate dibasic trihydrate ($K_2HPO_4 \cdot 3H_2O$), magnesium chloride hexahydrate ($MgCl_2 \cdot 6H_2O$), and calcium chloride ($CaCl_2$) all from CTR Scientific, sodium chloride (NaCl) from Omnichem, sodium sulfate (Na_2SO_4, anhydrous) from J. T. Baker, tris(hydroxymethyl) aminomethane ($(CH_2OH)_3CNH_2$) from Sigma-Aldrich, and hydrochloric acid (HCl) from Meyer were used for preparing SBF solution.

Deionized (DI) water (18.2 MΩcm, Millipore) was used for the preparation of solutions. All chemicals were utilized as received without further purification or processing.

Synthesis of Gold Nanoparticles. Monodispersed Au NPs used as cores in core@shell NPs were fabricated through a successive seed-mediated growth process, following the procedure reported by Zheng et al.[28] First, nanometric Au clusters were prepared by chemical reduction of $HAuCl_4$ using $NaBH_4$ as the reducing agent and CTAB as the stabilizing agent. In brief, 600 μL of a freshly prepared aqueous solution of $NaBH_4$ (10 mM) was quickly added to 10 mL of an aqueous solution of CTAB (100 mM) and $HAuCl_4$ (0.25 mM) mixture, resulting in a brownish solution. Then, for the synthesis of Au NPs of ca. 10 nm average diameter, 2 mL of an aqueous solution of $HAuCl_4$ (0.5 mM) was rapidly added to 22 mL of aqueous solutions of CTAC (18.8 mM) containing 1.5 mL of AA (100 mM) and 50 μL of the freshly prepared Au cluster solution under magnetic stirring, resulting in a yellowish mixture. The solution color gradually turned from yellowish to red. The product was centrifuged twice at 10 000 rpm for 1 h and redispersed in 1 mL of an aqueous CTAC solution (20 mM). Finally, to increase the size of the previously synthesized Au NPs to ca. 50 nm, 40 mL of an aqueous $HAuCl_4$ solution (5 mM) was slowly injected (20 mL/h) to an aqueous CTAC solution (200 mM) containing 3.24 mL of an AA solution (100 mM) and 150 μL of the as-prepared colloid of Au NPs (ca. 10 nm). During $HAuCl_4$ solution injection, the color of the colloid solution gradually turned from red to purple. The injection process was stopped when the solution color changed suddenly to deep translucent red. The product was centrifuged twice at 3000 rpm for 15 min and redispersed in 5 mL of an aqueous CTAC solution (25 mM). The whole synthesis process was performed at room temperature.

Fabrication of the SiO_2 Shells. Silica shells were fabricated over the as-prepared Au NPs (ca. 50 nm) using the Stöber method[20] assisted by ultrasonication. Prior to SiO_2 shell fabrication, the Au NPs were functionalized with mPEG-t and transferred to ethanol. For that, 10 mL of a colloidal Au solution ($[Au^0]$ = 0.5 mM) was centrifuged twice and redispersed in an aqueous CTAC solution (1.0 mM) of the same volume. Then, 0.5 mg of mPEG-t diluted in 1.5 mL of DI water was added dropwise to the colloid under vigorous stirring and left overnight under moderated stirring. After 12 h, the colloid was centrifuged twice and redispersed in 10 mL of ethanol. All centrifugation steps were performed at 3000 rpm for 15 min. mPEG-t binds strongly to the surface of the NPs via metal−S bonding, providing stability to the Au NPs in ethanol. On the contrary, the polymer chains over the Au NP surface have a good chemical affinity for TEOS.

For the synthesis of the silica shells, two solutions were prepared separately. The first solution (solution 1) was prepared by mixing 2.5 mL of the ethanol solution of Au NPs, 1.35 mL of DI water, and 100 μL of NH_4OH in 3.75 mL of ethanol. The second solution (solution 2) was prepared by adding 50 μL of TEOS to 7.4 mL of ethanol. Then, 300 μL of solution 2 was added to solution 1. The reaction mixture was kept under ultrasonic treatment (37 kHz, 80 W) for 2 h, maintaining the temperature of the water bath fixed at 20 °C. After that period, the solution was centrifuged twice at 3000 rpm for 15 min with ethanol; finally, the product was redispersed in 1.5 mL of ethanol for characterization. Another sample was prepared following the same procedure but keeping the water temperature of the ultrasonic bath at 40 °C. Two control samples were also prepared at 20 and 40 °C without ultrasonic treatment. The prepared samples were designated as $AuSiO_2$_20 (at 20 °C without US treatment), $AuSiO_2$_40 (at 40 °C without US treatment), $AuSiO_2$_US_20 (at 20 °C with US treatment), and $AuSiO_2$_US_40 (at 40 °C with US treatment). An ultrasonic bath from Elma Schmidbauer (s30 Elmasonic) was used during the silica layer growth (modified Stöber method) over the prefabricated Au NPs. The temperature of the ultrasonic-bath (containing water) was controlled by a refrigerated recirculating bath.

Chemical Stability Test. The chemical stability (resistance toward decomposition through hydrolysis) of the silica shells formed over the Au NPs was assessed through the standard test as described by Wong et al.[24] In brief, 0.5 mL of the Au@SiO_2 colloid was poured in 1.5 mL of DI water and heated to 90 °C for 24 h.

The stability of the composite structures was further tested in SBF at average body temperature (37 °C). The SBF was prepared following the procedure reported by Uribe-Madrid et al.[29] In brief, 350 mg of $NaHCO_3$, 224 mg of KCl, 228 mg of K_2HPO_4, 305 mg of $MgCl_2$, 278 mg of $CaCl_2$, 71 mg of Na_2SO_4, 7.99 g of NaCl, and 6.06 g of $(CH_2OH)_3CNH_2$ were all dissolved in 500 mL of DI water. Then, 40 mL of 1 M HCl was added to the mixture solution. The total volume of the

DOI: 10.1021/acs.jpcc.7b00933
J. Phys. Chem. C 2017, 121, 9543−9551

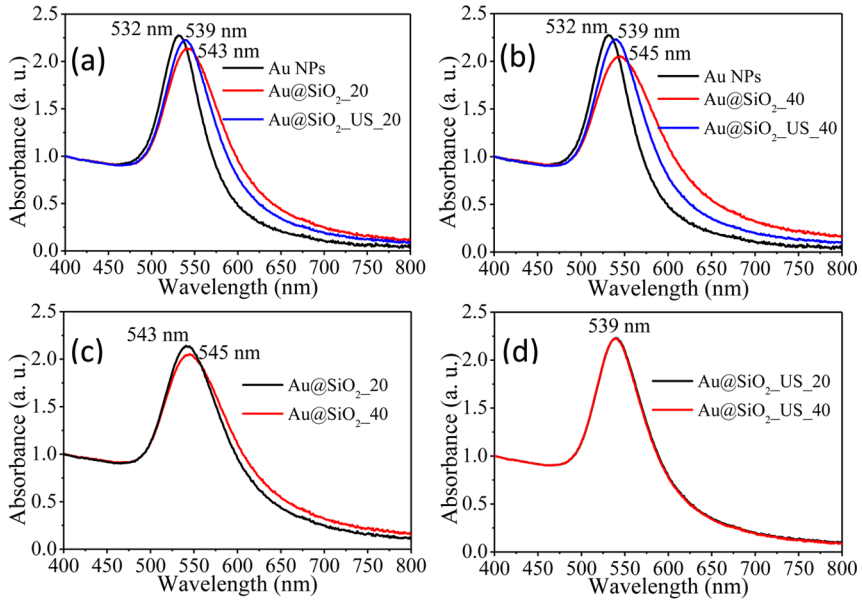

Figure 4. Absorption spectra of the (a) Au@SiO_2_20 and Au@SiO_2_US_20 and (b) Au@SiO_2_40 and Au@SiO_2_US_40 samples compared with those of bare Au NPs. Absorption spectra of the (c) Au@SiO_2_20 and Au@SiO_2_40 and (d) Au@SiO_2_US_20 and Au@SiO_2_US_40 samples. The spectra were normalized at 400 nm.

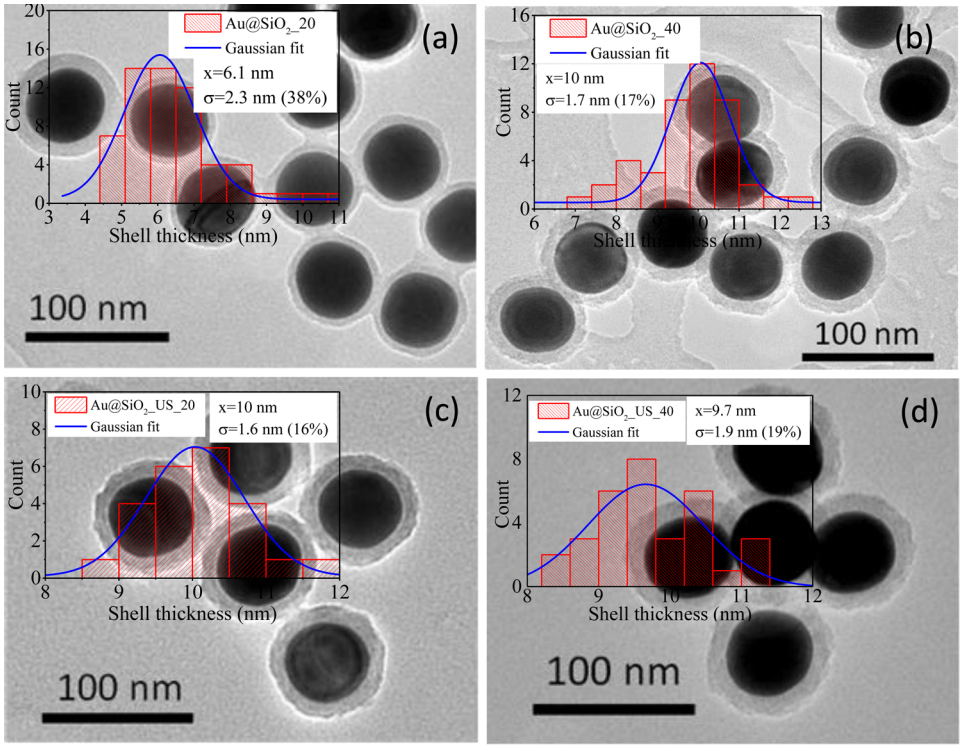

Figure 5. Typical TEM images and shell-thickness distribution histograms (insets) for the (a) Au@SiO_2_20, (b) Au@SiO_2_40, (c) Au@SiO_2_US_20, and (d) Au@SiO_2_US_40 samples.

mixture was adjusted to ca. 1 L by adding DI water so that the final solution had pH 7.4.

Characterization. The absorption spectra of the gold and silica-coated gold colloids were recorded in a Genesys 10S (Thermo Scientific) UV−vis spectrophotometer in the wavelength range from 400 to 800 nm in 0.5 nm steps. Apart from monitoring the position of the SPR band, the absorption spectra were utilized to theoretically calculate the average size of the colloidal NPs before and after silica shell fabrication. A JEOL JEM 1010 transmission electron microscope (TEM) was used to obtain images of the as-synthesized Au and Au@SiO_2 NPs, which were used to determine the NP morphology and their size distribution. Infrared transmittance spectra of the dry samples were recorded in the 650−4000 cm^{-1} range using a PerkinElmer 100 FTIR spectrometer, equipped with a universal ATR sampling accessory. For FTIR measurements, Au@SiO_2 colloids were dried at room temperature for 1 h after their separation from ethanol by centrifugation.

DOI: 10.1021/acs.jpcc.7b00933
J. Phys. Chem. C 2017, 121, 9543−9551

RESULTS AND DISCUSSION

The absorption spectrum of the as-synthesized Au NPs (Figure 3a) presents the characteristic SPR absorption band of spherical Au particles with a maximum at 532 nm. The experimental absorption spectrum was fitted to the absorption spectrum calculated by Mie-Lab,[30] a Mie-theory-based simulation program. The average particle size estimated from the theoretical fitting was 52.0 ± 1.7 nm. The formation of spherical shaped uniform gold particles in the sample is clear from the TEM image presented in Figure 3b. The size distribution histogram of the NPs (inset of Figure 3b), obtained by measuring their sizes from TEM images, revealed an average size of 52.8 ± 1.7 nm (3% size dispersion), which is very close to the average size value estimated through the theoretical fitting of the absorption spectrum of the sample.

The absorption spectra of the four Au@SiO_2 samples were recorder after their synthesis. The spectra of the samples prepared at 20 and 40 °C (with and without ultrasound treatment) are presented in Figure 4a,b, respectively. Absorption intensities of all spectra were normalized at 400 nm, where the absorption is mainly due to interband transitions of gold atoms, to facilitate their comparison, as the concentration of gold in all of the solutions was maintained same.[31] In general, the position of the SPR band for all samples shifted to longer wavelengths with respect to that of the bare NPs, indicating the formation of SiO_2 shells around the Au NPs. Nevertheless, the shift of the SPR band position for the samples prepared without ultrasound treatment is larger than that observed for the samples prepared with ultrasound treatment. Furthermore, their absorption bands are wider and less intense. These changes in the absorption bands are the possible consequences of the formation of thicker silica shells or the enclosure of more than one Au NP in single silica shell.[27] The increase in absorbance in the longer wavelength region of the absorption spectra of the NPs prepared without US treatment is due to their higher light scattering ability, indicative of a possible increase in size[32] (see Figure S1 of the Supporting Information) or agglomeration of the NPs.[33]

To demonstrate the effect of reaction temperature on silica shell growth, the absorption spectra of the samples fabricated without US treatment at 20 and 40 °C are presented in Figure 4c. The position of the SPR band shifts toward longer wavelength for the sample prepared at 40 °C, probably due to the growth of a thicker silica shell. On the contrary, the samples fabricated with US treatment have identical absorption spectra (Figure 4d) regardless of the reaction temperature, demonstrating that the thicknesses of the silica shells in both the samples are very similar.

Typical TEM images of all four silica-covered colloidal gold samples presented in Figure 5 confirm the formation of silica shells over Au NPs. Both the US treatment and temperature of reaction play important roles for controlling shell thickness and agglomeration of the Au@SiO_2 NPs. As can be seen in Figures 5a,b, the samples synthesized without US treatment, Au@SiO_2_20 and Au@SiO_2_40, have shell thicknesses of 6.1 ± 2.3 and 10 ± 1.7 nm, respectively. Increasing the reaction temperature yields a thicker shell due to an increase in TEOS hydrolysis and condensation rates.[34] However, agglomeration of Au@SiO_2 NPs is observed in the both samples due to interlinking of the silica shells of nearby NPs associated with their chemical instability. Agglomeration of Au@SiO_2 NPs enhances the interaction between their surface plasmons and hence shifts their SPR band position toward higher wavelengths in their absorption spectra, as has been observed for the samples fabricated without US treatment (Figure 4a,b). On the contrary, the samples synthesized using US treatment, Au@SiO_2_US_20 (Figure 5c) and Au@SiO_2_US_40 (Figure 5d), present a similar shell thickness (10 ± 1.6 and 9.7 ± 1.9 nm, respectively), indicating that the temperature is not a key parameter for controlling silica shell thickness when the reaction is performed under ultrasonic treatment. A good dispersion of Au@SiO_2 NPs is expected in this case, as the particles are in constant movement during ultrasonication.

The chemical stability of the silica shells in Au@SiO_2 structures was tested by heating them to 90 °C in DI water for 24 h. The TEM images of the samples are presented in Figure 6. By comparing these TEM images (Figure 6) of the samples with the corresponding TEM images before thermal hydrolysis (Figure 5), it is very clear that ultrasound treatment during shell formation improves the chemical stability of silica shells, avoiding their further hydrolysis and dissolution. As can be noticed, the silica shells of the AuSiO_2_20 (Figure 6a) and AuSiO_2_40 (Figure 6b) samples have almost completely dissolved on treating them in hot water. On the contrary, although the thickness of the silica shells of the AuSiO_2_US_20 (shell thickness of 2.9 ± 0.5 nm, Figure 6c) and AuSiO_2_US_40 (shell thickness of 6.9 ± 0.9 nm, Figure 6d) samples reduced a bit (70 and 28% of shell thickness reduction, respectively), the shells are not completely dissolved under the standard thermal hydrolysis test conditions. Moreover, the effect of hydrothermal etching is minimum for the sample AuSiO_2_US_40 (Figure 6d).

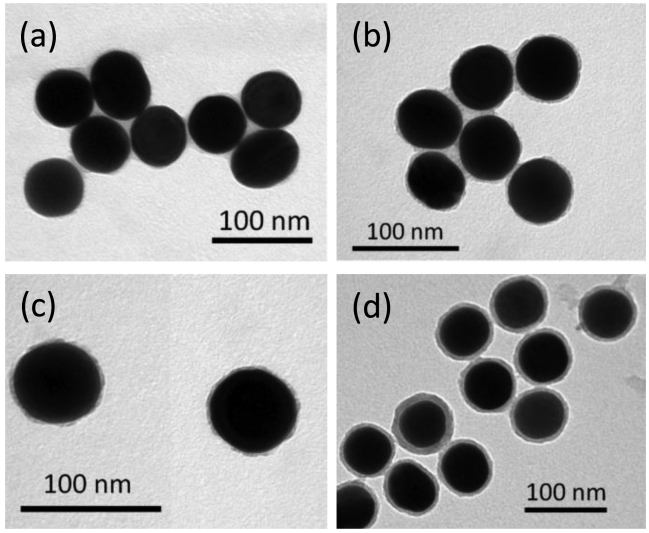

Figure 6. Typical TEM images of the (a) Au@SiO_2_20, (b) Au@SiO_2_40, (c) Au@SiO_2_US_20, and (d) Au@SiO_2_US_40 samples after hydrothermal etching test.

Room-temperature FTIR spectra of Au@SiO_2 samples (Figure 7) were recorded to determine the quality of their SiO_2 shells. The FTIR spectra of all samples revealed several sharp, well-defined absorption bands in the measured spectral range (400−4000 cm^{-1}). The bands centered at 792, 1061, and 1200 cm^{-1} (shoulder) are the stretching vibrations of siloxane groups,[35,36] while the band revealed around 950 cm^{-1} corresponds to the stretching vibration of silanol groups in the silica lattice[36−38] (see Table S1 of Supporting Information).

DOI: 10.1021/acs.jpcc.7b00933
J. Phys. Chem. C 2017, 121, 9543−9551

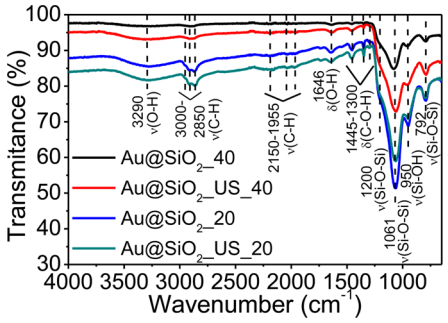

Figure 7. Infrared transmission spectra of the fabricated Au@SiO_2 samples.

The bands appeared at 1300 cm^{-1}, and higher frequencies are attributed to the vibrational modes of ethanol molecules[37] adsorbed at the surface of the samples (Table S1). The presence of 950 cm^{-1} absorption band in the FTIR spectra indicates the silica shells of all samples contain a considerable amount of silanol groups, either at their surface or in the shell pores as terminal bonds (Figure 2).

Because the quality of the silica shells formed over Au NPs depends strongly on the relative concentration of siloxane groups with respect to silanol groups, we estimated the intensity ratio between the most prominent absorption band associated with siloxane groups and the absorption band of the silanol groups appeared at 950 cm^{-1}. For that, we first deconvoluted the absorption spectra of all samples in the 700−1300 cm^{-1} spectral range, using five Gaussian sub-bands, in which the shoulder at 1200 cm^{-1} (Figure 7) consisted of two sub-bands centered at around 1215 and 1157 cm^{-1}.[36] The bands obtained from the deconvolution of the IR absorption spectra (green lines), their sum (red line), and the experimental spectra (black line) of the Au@SiO_2 samples are shown in Figure 8. As the band around 1068 cm^{-1}, which corresponds to the transverse optical (TO) asymmetric stretching vibration of Si−O−Si, appeared to be the most intense among the deconvoluted components, its intensity was compared with

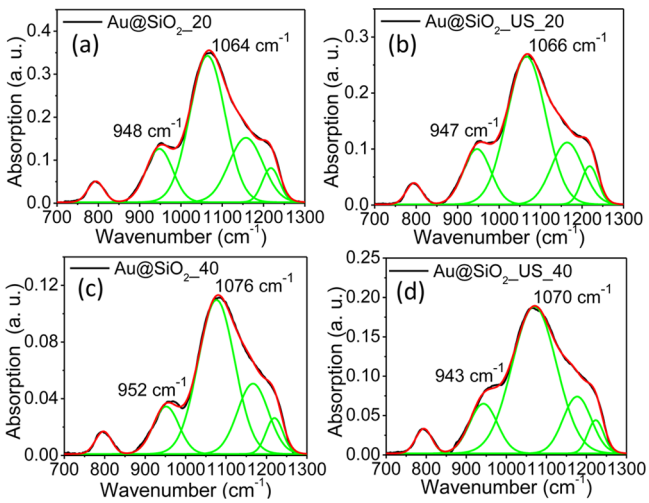

Figure 8. Deconvoluted IR absorption spectra of the dry (a) Au@SiO_2_20, (b) Au@SiO_2_US_20, (c) Au@SiO_2_40, and (d) Au@SiO_2_US_40 samples in the 700−1300 cm^{-1} spectral range. The most intense and confirmative bands appeared between 1064 and 1076 cm^{-1}, and the band between 943 and 952 cm^{-1} was used to calculate the intensity ratio of ν(Si−O−Si) and ν(Si−OH) (Table 1).

the intensity of the stretching vibrational mode of silanol at 950 cm^{-1}.[39] The estimated intensity ratios (I_{Si-O}/I_{Si-OH}) for the four samples are presented in Table 1. Because the presence of a higher amount of siloxane groups would make the silica network more stable,[24,40] a larger intensity ratio (I_{Si-O}/I_{Si-OH}) would indicate a better quality (higher stability) of the silica shell. We can see from Table 1 that an increase in the reaction temperature during silica shell formation increases the siloxane/silanol ratio, that is, the silica shell quality, irrespective of the ultrasound treatment. On the contrary, the quality of the silica shells prepared with ultrasonic treatment is much better than the shells fabricated without US treatment. The nonstoichiometric composition of smaller particles, and its improvement with particle size has also been noticed by Leite et al.[41] for their silica NPs fabricated by conventional Stöber method.

To understand the mechanism of degradation of the silica shells formed over metal NPs through the conventional Stöber method, we must remember that the hydrolyzed derivatives of TEOS ($Si(OH)_n$) are soluble in water.[40] Depending on the extent of condensation, they can form network structures where a Si atom is coordinated to four oxygen atoms (i.e., containing only siloxane bonds) or networks where some of the Si atoms are attached to hydroxyl groups (i.e., containing silanol bonds). If all Si atoms of the network are coordinated only to oxygen atoms, then the structure is chemically stable and protected from further hydrolysis at room temperature (Figure 9a). However, if some of the Si atoms of the network are coordinated to hydroxyl groups, as shown in Figure 9b, they are prone to further hydrolysis and hence the shell is unstable. At high temperatures, the concentrations of hydroxyl groups and protons (H^+) in water increase.[42] On treating the silica network containing both siloxane and silanol bonds in hot water, the siloxane (Si−O−Si) bonds break down to form silanol (Si−OH) bonds, which coordinate to the OH^- ions of hot water. Because the Si−O bonds are of polar-covalent nature owing to the high electronegativity difference between the Si (1.9) and oxygen (3.44) atoms,[43] the hydroxyl ions of hot water react with the Si atoms of positive charge density (δ^+) through electrostatic interaction (Figure 9c). Although the same phenomenon of bond breaking can also occur in a silica network containing only siloxane bonds, a higher amount of energy is needed for this to happen. As the water ionization rate and the diffusion rate of ions (OH^- and H^+) increase with temperature, the hydrolysis rate of silica also increases at higher temperatures. This is the reason behind using hot water for the standard stability test on silica shells.

If the silica shells are not well formed or not stoichiometric, that is, there are many silanol groups, as depicted in Figure 9b, they will dissolve in hot water at a faster rate, as has been observed for the samples prepared without US treatment. On the contrary, the samples prepared under ultrasonication are more resistant to further hydrolysis (Figure 9a), and hence their silica shells do not dissolve under the performed standard test.

To verify the stability of the fabricated Au@SiO_2 NPs under biological conditions, the sample Au@SiO_2_US_20 fabricated under ultrasonication was tested in SBF solution at 37 °C for 1.5 days (36 h). The test was performed by centrifuging 1.5 mL of the as-synthesized colloidal sample and redispersing the composite NPs in a glass vial containing 5 mL of SBF solution at 37 °C. After 36 h of SBF treatment at 37 °C, the NPs in colloidal solution were characterized by UV−vis absorption spectroscopy and TEM and compared with the results obtained before their SBF treatment. The 36 h time of SBF treatment

DOI: 10.1021/acs.jpcc.7b00933
J. Phys. Chem. C 2017, 121, 9543−9551

Table 1. Intensity Ratio of the Si−O−Si and Si−OH Vibrational Modes (I_{Si-O}/I_{Si-OH}) for the Au@SiO_2 Samples Estimated from Their Infrared Absorption Spectra

sample	position of Si−OH mode (cm^{-1})	intensity of Si−OH mode (I_{Si-OH})	position of Si−O−Si mode (cm^{-1})	intensity of Si−O−Si mode (I_{Si-O})	I_{Si-O}/I_{Si-OH}
Au@SiO_2_20	948	10	1064	36.4	3.64
Au@SiO_2_US_20	947	8.2	1066	30.8	3.76
Au@SiO_2_40	952	2.7	1076	12.3	4.56
Au@SiO_2_US_40	943	5.5	1070	26	4.73

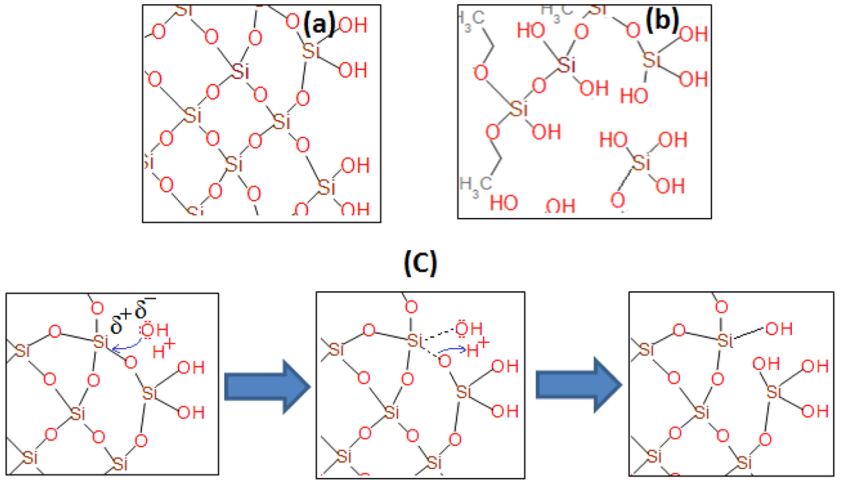

Figure 9. Schematic presentation of the silica structures formed over Au NPs (a) without and (b) with ultrasonic treatment. (c) Schematic representation of the thermal hydrolysis of silica containing siloxane bonds.

was considered in this study because the time is longer than the reported blood half-life of gold NPs covered with other materials.[44]

As can be observed from the absorption spectra presented in Figure 10, the position of the SPR band of the sample did not

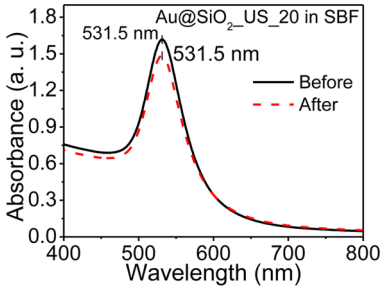

Figure 10. Absorbance spectra of the colloidal Au@SiO_2_US_20 sample in SBF before (black line) and after (dashed red line) SBF treatment at 37 °C for 36 h.

change after SBF treatment. However, the absorption intensity in the longer wavelength range (>620 nm) increased slightly with respect to the intensity of the SPR band. This increase in relative intensity of absorption at higher wavelength region (increased light scattering) might be due to change in surface morphology, that is, surface roughness[45] of the silica shell due to SBF treatment, or an agglomeration of NPs.[33]

Representative TEM images of the sample before and after SBF treatment are presented in Figures 11 and 12, respectively. As can be seen, the NPs conserve their silica shell after 36 h of SBF treatment. However, the thickness of the silica shells of some of the composite particles is reduced, from 6.4 ± 1.7 to 5.2 ± 1.5 nm, and some of the NPs are agglomerated.

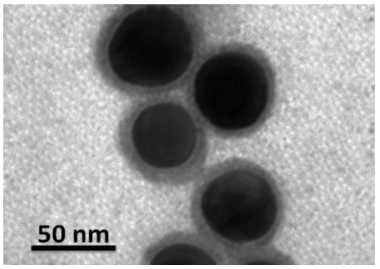

Figure 11. Typical TEM image of the Au@SiO_2_US_20 sample before SBF treatment.

Nevertheless, the shell thickness reduction during SBF treatment (~19%) is much lower than reduction (~70%) that occurred by hydrothermal treatment, even though the treatment time was much longer in the former case. As has been previously described, temperature is the main parameter that controls the rate of hydrolysis and hence the shell degradation process.

While a mild agglomeration of the composite particles occurs during SBF treatment due to the bonding of the silanol groups and dangling bonds at the surface of the silica shells, it has no significant effect on the absorption spectrum of the sample. The results presented above indicate the Au@SiO_2 NPs fabricated under sonication are reasonably stable in human body fluid (blood), the medium through which they can be introduced for biomedical applications.

Finally, we must mention that although ultrasound assisted Stöber method has been utilized by several research groups to fabricate spherical silica NPs of uniform sizes,[46,47] rare-earth doped spherical silica NPs,[38] and other silica coated nanostructures,[48] none have tested or discussed their stability in hydrolyzing media such as in hot water or in body fluids.

DOI: 10.1021/acs.jpcc.7b00933
J. Phys. Chem. C 2017, 121, 9543−9551

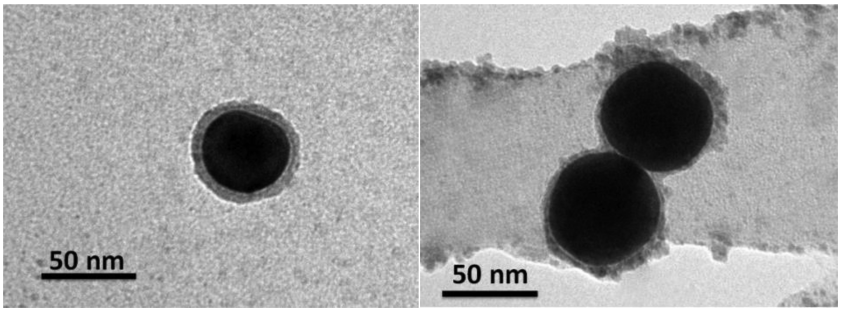

Figure 12. Typical TEM images of the colloidal Au@SiO_2_US_20 sample after SBF treatment at 37 °C for 36 h.

CONCLUSIONS

We could fabricate stable, thin silica shell layers over plasmonic metal NPs such as Au through ultrasonication during Stöber process. The ultrasound treatment during silica shell growth accelerates both the hydrolysis of TEOS and the condensation of $Si(OH)_4$ monomers, reducing the concentration of silanol groups in the formed silica lattice. Although an increase in the temperature during silica shell growth also enhances the TEOS hydrolysis and $Si(OH)_4$ condensation rates, the utilization of the ultrasound treatment helps to maintain the silica-coated metal NPs dispersed, avoiding their agglomeration. The silica layers formed over Au NPs at 40 °C with ultrasonication possess better stoichiometry and are resistant to degradation in aqueous media even at 90 °C. The silica-coated Au NPs are reasonably stable in SBF at 37 °C for 36 h. Such stable, monodispersed core−shell plasmonic nanostructures are very useful for biomedical applications, where the surrounding media could be aggressive to bare metallic NPs. The method utilized to fabricate stable Au@SiO_2 NPs in this work could be extended for fabricating other metal@SiO_2 nanostructures.

ASSOCIATED CONTENT

Supporting Information

The Supporting Information is available free of charge on the ACS Publications website at DOI: 10.1021/acs.jpcc.7b00933.

Table S1. Observed IR bands of the four Au@SiO_2 samples and their mode assignation. (PDF)

AUTHOR INFORMATION

Corresponding Authors

*A.G.-M.: E-mail: aguerrero@quim.ucm.es. Fax: +34-91-3944136.

*U.P.: E-mail: upal@ifuap.buap.mx. Fax: +52-222-2295611.

ORCID

Andrés Guerrero-Martínez: 0000-0001-8576-2896

Ovidio Peña-Rodríguez: 0000-0002-7329-0550

Umapada Pal: 0000-0002-5665-106X

Author Contributions

The manuscript was written through contributions from all authors. All authors have approved the final version of the manuscript.

Notes

The authors declare no competing financial interest.

ACKNOWLEDGMENTS

The work was financially supported by CONACyT, Mexico (Becamixta no. 290936), VIEP-BUAP (VIEP/EXC/2017), and DITCo-BUAP (DITCo/2016-13). We thank the Laboratorio Nacional de Supercómputo del Sureste (LNS), BUAP, Mexico, for providing computing resources to perform theoretical calculations.

REFERENCES

(1) Gangishetty, M. K.; Lee, K. E.; Scott, R. W. J.; Kelly, T. L. Plasmonic Enhancement of Dye Sensitized Solar Cells in the Red-to Near-Infrared Region using Triangular Core−Shell Ag@SiO_2 Nanoparticles. *ACS Appl. Mater. Interfaces* **2013**, *5*, 11044−11051.

(2) Liu, W.-L.; Lin, F.-C.; Yang, Y.-C.; Huang, C.-H.; Gwo, S.; Huang, M. H.; Huang, J.-S. The Influence of Shell Thickness of Au@TiO_2 Core−Shell Nanoparticles on the Plasmonic Enhancement Effect in Dye-Sensitized Solar Cells. *Nanoscale* **2013**, *5*, 7953−7962.

(3) Wooh, S.; Lee, Y.-G.; Tahir, M. N.; Song, D.; Meister, M.; Laquai, F.; Tremel, W.; Bisquert, J.; Kang, Y. S.; Char, K. Plasmon-Enhanced Photocurrent in Quasi-Solid-State Dye-Sensitized Solar Cells by the Inclusion of Gold/Silica Core−Shell Nanoparticles in a TiO_2 Photoanode. *J. Mater. Chem. A* **2013**, *1*, 12627−12634.

(4) Tian, X.-D.; Liu, B.-J.; Li, J.-F.; Yang, Z.-L.; Ren, B.; Tian, Z.-Q. SHINERS and Plasmonic Properties of Au Core SiO_2 Shell Nanoparticles with Optimal Core Size and Shell Thickness. *J. Raman Spectrosc.* **2013**, *44*, 994−998.

(5) Yang, J.; Zhang, F.; Chen, Y.; Qian, S.; Hu, P.; Li, W.; Deng, Y.; Fang, Y.; Han, L.; Luqman, M.; Zhao, D. Core-shell Ag@SiO_2@mSiO_2 Mesoporous Nanocarriers for Metal-Enhanced Fluorescence. *Chem. Commun.* **2011**, *47*, 11618−11620.

(6) Ming, T.; Zhao, L.; Yang, Z.; Chen, H.; Sun, L.; Wang, J.; Yan, C. Strong Polarization Dependence of Plasmon-Enhanced Fluorescence on Single Gold Nanorods. *Nano Lett.* **2009**, *9*, 3896−3903.

(7) Tovmachenko, O. G.; Graf, C.; van den Heuvel, D. J.; van Blaaderen, A.; Gerritsen, H. C. Fluorescence Enhancement by Metal-Core/Silca-Shell Nanoparticles. *Adv. Mater.* **2006**, *18*, 91−95.

(8) Wang, K.; He, X.; Yang, X.; Shi, H. Functionalized Silica Nanoparticles: A Platform for Fluorescence Imaging at the Cell and Small Animal Levels. *Acc. Chem. Res.* **2013**, *46*, 1367−1376.

(9) Stober, W.; Fink, A.; Bohn, E. Controlled Growth of Monodisperse Silica Spheres in the Micron Size Range. *J. Colloid Interface Sci.* **1968**, *26*, 62−69.

(10) Reineck, P.; Gómez, D.; Ng, S. H.; Karg, M.; Bell, T.; Mulvaney, P.; Bach, U. Distance and Wavelength Dependent Quenching of Molecular Fluorescence by Au@SiO_2 Core Shell Nanoparticles. *ACS Nano* **2013**, *7*, 6636−6648.

(11) Brinker, C. J.; Scherer, G. W. *Sol-Gel Science: The Physics and Chemistry of Sol-Gel Processing*; Academic Press: San Diego, 1990; pp 1−18.

(12) Li, J. F.; Huang, Y. F.; Ding, Y.; Yang, Z. L.; Li, S. B.; Zhou, X. S.; Fan, F. R.; Zhang, W.; Zhou, Z. Y.; Wu, D. Y.; Ren, B.; Wang, Z. L.; Tian, Z. Q. Shell-Isolated Nanoparticle-Enhanced Raman Spectroscopy. *Nature* **2010**, *464*, 392−395.

(13) Hembury, M.; Chiappini, C.; Bertazzo, S.; Kalber, T. L.; Drisko, G. L.; Ogunlade, O.; Walker-Samuel, S.; Krishna, K. S.; Jumeaux, C.; Beard, P.; et al. Gold−Silica Quantum Rattles for Multimodal Imaging and Therapy. *Proc. Natl. Acad. Sci. U. S. A.* **2015**, *112*, 1959−1964.

DOI: 10.1021/acs.jpcc.7b00933
J. Phys. Chem. C 2017, 121, 9543−9551

(14) Aznar, E.; Marcos, M. D.; Martínez-Máñez, R.; Sancenón, F.; Soto, J.; Amorós, J.; Guillem, C. pH- and Photo-Switched Release of Guest Molecules from Mesoporous Silica Supports. *J. Am. Chem. Soc.* **2009**, *131*, 6833−6843.
(15) Liu, J.; Detrembleur, C.; De Pauw-Gillet, M. C.; Mornet, S.; Jérôme, C.; Duguet, E. Gold Nanorods Coated with Mesoporous Silica Shell as Drug Delivery System for Remote Near Infrared Light-Activated Release and Potential Phototherapy. *Small* **2015**, *11*, 2323−32.
(16) Fang, P. P.; Li, J. F.; Yang, Z. L.; Li, L. M.; Ren, B.; Tian, Z. Q. Optimization of SERS Activities of Gold Nanoparticles and Gold-Core−Palladium-Shell Nanoparticles by Controlling Size and Shell Thickness. *J. Raman Spectrosc.* **2008**, *39*, 1679−1687.
(17) Montaño-Priede, L.; Peña-Rodríguez, O.; Rivera, A.; Guerrero-Martínez, A.; Pal, U. Optimizing the Electric Field Around Solid and Core−Shell Alloy Nanostructures for Near-Field Applications. *Nanoscale* **2016**, *8*, 14836−14845.
(18) Liz-Marzán, L. M.; Giersig, M.; Mulvaney, P. Synthesis of Nanosized Gold-Silica Core-Shell Particles. *Langmuir* **1996**, *12*, 4329−4335.
(19) Mulvaney, S. P.; Musick, M. D.; Keating, C. D.; Natan, M. J. Glass-Coated, Analyte-Tagged Nanoparticles: A New Tagging System Based on Detection with Surface-Enhanced Raman Scattering. *Langmuir* **2003**, *19*, 4784−4790.
(20) Fernández-López, C.; Mateo-Mateo, C.; Álvarez-Puebla, R. A.; Pérez-Juste, J.; Pastoriza-Santos, I.; Liz-Marzán, L. M. Highly Controlled Silica Coating of PEG-Capped Metal Nanoparticles and Preparation of SERS-Encoded Particles. *Langmuir* **2009**, *25*, 13894−13899.
(21) Mine, E.; Yamada, A.; Kobayashi, Y.; Konno, M.; Liz-Marzán, L. M. Direct Coating of Gold Nanoparticles with Silica by a Seeded Polymerization Technique. *J. Colloid Interface Sci.* **2003**, *264*, 385−390.
(22) Graf, C.; van Blaaderen, A. Metallodielectric Colloidal Core-Shell Particles for Photonic Applications. *Langmuir* **2002**, *18*, 524−534.
(23) Graf, C.; Vossen, D. L. J.; Imhof, A.; van Blaaderen, A. A General Method to Coat Colloidal Particles with Silica. *Langmuir* **2003**, *19*, 6693−6700.
(24) Wong, Y. J.; Zhu, L.; Teo, W. S.; Tan, Y. W.; Yang, Y.; Wang, C.; Chen, H. Revisiting the Stöber Method: Inhomogeneity in Silica Shells. *J. Am. Chem. Soc.* **2011**, *133*, 11422−11425.
(25) Zhang, Y.; Kong, X.; Xue, B.; Zeng, Q.; Liu, X.; Tu, L.; Liu, K.; Zhang, H. A Versatile Synthesis Route for Metal@SiO_2 Core−Shell Nanoparticles Using 11-Mercaptoundecanoic Acid as Primer. *J. Mater. Chem. C* **2013**, *1*, 6355−6363.
(26) Kobayashi, Y.; Katakami, H.; Mine, E.; Nagao, D.; Konno, M.; Liz-Marzán, L. M. Silica Coating of Silver Nanoparticles Using a Modified Stöber Method. *J. Colloid Interface Sci.* **2005**, *283*, 392−396.
(27) Vanderkooy, A.; Chen, Y.; Gonzaga, F.; Brook, M. A. Silica Shell/Gold Core Nanoparticles: Correlating Shell Thickness with the Plasmonic Red Shift upon Aggregation. *ACS Appl. Mater. Interfaces* **2011**, *3*, 3942−3947.
(28) Zheng, Y.; Zhong, X.; Li, Z.; Xia, Y. Successive, Seed−Mediated Growth for the Synthesis of Single−Crystal Gold Nanospheres with Uniform Diameters Controlled in the Range of 5−150 nm. *Part. Part. Syst. Charact.* **2014**, *31*, 266−273.
(29) Uribe-Madrid, S. I.; Pal, U.; Kang, Y. S.; Kim, J.; Kwon, H.; Kim, J. Fabrication of Fe_3O_4@mSiO_2 Core-Shell Composite Nanoparticles for Drug Delivery Applications. *Nanoscale Res. Lett.* **2015**, *10*, 217.
(30) Peña-Rodríguez, O.; González Pérez, P. P.; Pal, U. MieLab: A Software Tool to Perform Calculations on the Scattering of Electromagnetic Waves by Multilayered Spheres. *Int. J. Spectrosc.* **2011**, *2011*, 1.
(31) Rodríguez-Fernández, J.; Pérez-Juste, J.; García de Abajo, F. J.; Liz-Marzán, L. M. Seeded Growth of Submicron Au Colloids with Quadrupole Plasmon Resonance Modes. *Langmuir* **2006**, *22*, 7007−7010.
(32) Zhang, R.; Zhou, Y.; Peng, L.; Li, X.; Chen, S.; Feng, X.; Guan, Y.; Huang, W. Influence of SiO_2 Shell Thickness on Power Conversion Efficiency in Plasmonic Polymer Solar Cells with Au Nanorod@SiO_2 Core-Shell Structures. *Sci. Rep.* **2016**, *6* (1), 1−9.
(33) Bohren, C. F.; Huffman, D. R. *Absorption and Scattering of Light by Small Particles*; Wiley-Interscience: New York, 1998; pp 57−129.
(34) Kamiya, K.; Yoko, T.; Suzuki, H. Hydrolysis-Condensation Reaction of Tetraethylorthosilicate (TEOS) for Glass Fiber-Drawing: Effect of Reaction Temperature on the Type of Produced Siloxane Polymers. *J. Non-Cryst. Solids* **1987**, *93*, 407−414.
(35) Gunde, M. K. Vibrational Modes in Amorphous Silicon Dioxide. *Phys. B (Amsterdam, Neth.)* **2000**, *292*, 286−295.
(36) Bertoluzza, A.; Fagnano, C.; Morelli, M. A.; Gottardi, V.; Guglielmi, M. Raman and Infrared Spectra on Silica Gel Evolving Toward Glass. *J. Non-Cryst. Solids* **1982**, *48*, 117−128.
(37) Plyler, E. K. Infrared Spectra of Methanol, Ethanol, and n-Propanol. *J. Res. Natl. Bur. Stand.* **1952**, *48*, 281−286.
(38) Patra, A.; Sominska, E.; Ramesh, S.; Koltypin, Yu.; Zhong, Z.; Minti, H.; Reisfeld, R.; Gedanken, A. Sonochemical Preparation and Characterization of Eu_2O_3 and Tb_2O_3 Doped in and Coated on Silica and Alumina Nanoparticles. *J. Phys. Chem. B* **1999**, *103*, 3361−3365.
(39) Wang, S.; Wang, D. K.; Smart, S.; Diniz da Costa, J. C. Ternary Phase-Separation Investigation of Sol-Gel Derived Silica from Ethyl Silicate 40. *Sci. Rep.* **2015**, *5* (14560), 1−11.
(40) Unger, K. K. *Porous Silica*; J. Chromatogr. Library *16*; Elsevier, 1979.
(41) Leite, C. A. P.; de Souza, E. F.; Galembeck, F. Core-and-Shell Nature of Stöber Silica Particles. *J. Braz. Chem. Soc.* **2001**, *12*, 519−525.
(42) Chang, R. *Chemistry*, 9th ed.; McGraw-Hill: New York, 2007.
(43) Elias, H.-G. *Macromolecules*; Springer: New York, 1977; pp 1115−1122.
(44) Dreaden, E. C.; Austin, L. A.; Mackey, M. A.; El-Sayed, M. A. Size Matters: Gold Nanoparticles in Targeted Cancer Drug Delivery. *Ther. Delivery* **2012**, *3*, 457−478.
(45) Sánchez-Gil, J. A.; Nieto-Vesperinas, M. Light Scattering from Random Rough Dielectric Surfaces. *J. Opt. Soc. Am. A* **1991**, *8*, 1270−1286.
(46) Masjedi-Arani, M.; Salavati-Niasari, M.; Ghanbari, D.; nabiyouni, G. A Sonochemical-Assisted Synthesis of Spherical Silica Nanostructures by Using a New Capping Agent. *Ceram. Int.* **2014**, *40*, 495−499.
(47) Gholami, T.; Salavati-Niasari, M.; Bazarganipour, M.; Noori, E. Synthesis and Characterization of Spherical Silica Nanoparticles by Modified Stöber Process Assisted by Organic Ligand. *Superlattices Microstruct.* **2013**, *61*, 33−41.
(48) Liu, H.; Ji, S.; Yang, H.; Zhang, H.; Tang, M. Ultrasonic-Assisted Ultra-Rapid Synthesis of Monodisperse Meso-SiO_2@Fe_3O_4 Microspheres with Enhanced Mesoporous Structure. *Ultrason. Sonochem.* **2014**, *21*, 505−512.

DOI: 10.1021/acs.jpcc.7b00933
J. Phys. Chem. C 2017, 121, 9543−9551